

Novel flavour-changing neutral currents in the top quark sector

Nuno Castro^a, Mikael Chala^b, Ana Peixoto^a, Maria Ramos^a

^aLaboratório de Instrumentação e Física Experimental de Partículas,
Departamento de Física, Universidade do Minho,
4710-057 Braga, Portugal

^bCAFPE and Departamento de Física Teórica y del Cosmos,
Universidad de Granada, E18071 Granada, Spain

Abstract

We demonstrate that flavour-changing neutral currents in the top sector, mediated by leptophilic scalars at the electroweak scale, can easily arise in scenarios of new physics, and in particular in composite Higgs models. We moreover show that such interactions are poorly constrained by current experiments, while they can be searched for at the LHC in rare top decays and, more generally, in the channels $pp \rightarrow tS(S) + j$, with $S \rightarrow \ell^+\ell^-$. We provide dedicated analyses in this respect, obtaining that cut-off scales as large as $\Lambda \sim 90$ TeV can be probed with an integrated luminosity of $\mathcal{L} = 150$ fb⁻¹.

Keywords: rare decays, top quark, leptons, flavour-changing neutral currents

1 Introduction

New pseudoscalars S with mass m_S close to the electroweak (EW) scale, singlets of the Standard Model (SM) gauge group, have two opposing faces. On one hand, they are predicted in very different and well motivated scenarios of new physics. These include, among others, the NMSSM [1] in which an extra supersinglet reduces the μ -problem; as well as a big part of the composite Higgs models (CHM) developed to the date [2–15]. Moreover, pseudoscalar singlets have been showed to be excellent candidates to accommodate EW baryogenesis with two step phase transitions at which CP is spontaneously broken [10, 15–21]. Also, they have been proved to explain the $g - 2$ anomaly of the muon [22].

However, on the other hand, pseudoscalar singlets around the EW scale are very difficult to detect. The first reason is that at the renormalisable level they only interact with the Higgs boson. If they are above the threshold $\sim m_h/2$, they are therefore produced only with extremely low cross section by means of an off-shell Higgs; being even out of the reach of a potential 100 TeV collider [23]. Moreover, the strong constraints on dipole moments [24, 25] forbids any sizable mixing with the Higgs, while other production mechanisms are mediated by higher-dimensional operators and therefore suppressed by the cut-off scale [26, 27], that hereafter we refer as to Λ .

In light of these results, there has been research exploring novel production mechanisms for new pseudoscalar singlets. One of the most exciting possibilities is producing such particles in the decay of top quarks via effective interactions. Such proposal aims to exploit the huge top quark production rate at the Large Hadron Collider (LHC) and future facilities. Search strategies for $t \rightarrow Sq, S \rightarrow b\bar{b}(\gamma\gamma)$ have been discussed in Ref. [28]. (See Refs. [29–31] for studies focused on $m_S \sim m_h \sim 125$ GeV and Refs. [32, 33] for experimental works.) For $m_S \gtrsim m_t \sim 172$ GeV, the top quark decays non resonantly; being adequately described by four-fermion interactions [34].

In this article, we extend previous works in this topic in three ways. First, we consider the rare top decay $t \rightarrow Sq, S \rightarrow \ell^+\ell^-$ including both light leptons and taus. Second, we include the effect of the flavour-violating vertices not only in the decay, but also in the production of top quarks¹. And third, we demonstrate that a more natural new top decay is $t \rightarrow SS, S \rightarrow \ell^+\ell^-$ and we also study in detail the LHC reach to this process.

The text is organized as follows. In section 2 we introduce the relevant dimension-six effective field theory Lagrangian of the SM extended with S and compare to concrete models. We show which interactions are already constrained by current Higgs and flavour data, and define several benchmark points (BP) for the subsequent study of top decays. We dedicate sections 3 and 4 to explore the collider phenomenology of $t \rightarrow Sq$ with $S \rightarrow \ell^+\ell^-$ and $S \rightarrow \tau^+\tau^-$, respectively. In section 5 we concentrate on $t \rightarrow SSq, S \rightarrow \ell^+\ell^-$. We conclude in section 6.

¹The interference effects between the production and decay modes were shown to be negligible in Ref. [35].

2 Interactions and constraints

The most generic Lagrangian describing the interactions (that can be induced at tree level in UV completions of the SM to dimension six) between a scalar singlet S with mass m_S and the SM fields reads [26]:

$$\begin{aligned} \Delta L = & -\frac{1}{2}\lambda_{HS}S^2\left(|H|^2 - \frac{v^2}{2}\right) + c_{HS}\frac{(\partial S)^2}{\Lambda^2}|H|^2 \\ & + \frac{S}{\Lambda}\bar{\mathbf{f}}_{\mathbf{L}}\mathbf{Y}^{\mathbf{f}}H\mathbf{f}_{\mathbf{R}} + \frac{S^2}{\Lambda^2}\left[c'_{HS}|DH|^2 + \tilde{c}_{HS}\left(|H|^4 - \frac{v^4}{4}\right) + \bar{\mathbf{f}}_{\mathbf{L}}\tilde{\mathbf{Y}}^{\mathbf{f}}H\mathbf{f}_{\mathbf{R}}\right]. \end{aligned} \quad (1)$$

(The addition of the hermitian conjugate in the fermions, as well as $\tilde{H} = i\sigma_2 H^*$ when needed, is implied; with H being the Higgs doublet and σ_2 the second Pauli matrix.) We note that f runs over quarks and leptons, $f = q, l$. Let us work in the approximation that the CabibboKobayashiMaskawa matrix is fully diagonal, then no rotation is needed on $\mathbf{f}_{\mathbf{L},\mathbf{R}}$. The different Wilson coefficients in the expression above are subject to a number of constraints. Thus, λ_{HS} , c_{HS} and \tilde{c}_{HS} enter the Higgs width:

$$\Gamma(h \rightarrow SS) = \frac{1}{32\pi m_h} \sqrt{1 - \frac{4m_S^2}{m_h^2}} \left[\lambda_{HS} + c_{HS} \frac{(m_h^2 - 2m_S^2)}{\Lambda^2} - 2\tilde{c}_{HS} \frac{v^2}{\Lambda^2} \right]^2. \quad (2)$$

Therefore, values of $m_S < m_h/2$ are *a priori* constrained by LHC measurements on the Higgs width, $\Gamma_H \lesssim 10$ MeV [36]. This bound can be evaded only if cancellations between the different operators in the bracket make this smaller than ~ 0.05 . Assuming one operator at a time, we obtain the bounds $\lambda_{HS} \lesssim 0.05$; $c_{HS}/\Lambda^2 \lesssim 3(5)$ TeV⁻² for $m_S = 10(50)$ GeV; and $-\tilde{c}_{HS}/\Lambda^2 \lesssim 0.4$ TeV⁻².

Entries in $\mathbf{Y}^{\mathbf{f}}$ and $\tilde{\mathbf{Y}}^{\mathbf{f}}$ are constrained by *e.g.* direct searches for resonances [37, 38]. One important exception is entries $i3, 3i$ of $\mathbf{Y}^{\mathbf{q}}$. There are no direct limits on these. Moreover, indirect constraints from flavour experiments, *e.g.* $D^0 - \bar{D}^0$ oscillations [39–41], involve always products of two different Yukawas. They are therefore negligible if *e.g.* the entry 13 or 23 of $\mathbf{Y}^{\mathbf{q}}$ vanishes [28]; same for $\tilde{\mathbf{Y}}^{\mathbf{q}}$. However, they can be observable in new experiments. Indeed, after EWSB and for $m_t > m_S (2m_S)$, they lead to signatures such as $t \rightarrow qS(S)$ arising from

$$\Delta L \supset \frac{vS}{\sqrt{2}\Lambda} \left[\mathbf{Y}^{\mathbf{q}}_{i3} \bar{u}_L^i t_R + \mathbf{Y}^{\mathbf{q}}_{3i} \bar{t}_L u_R^i + \frac{S}{\Lambda} \left(\tilde{\mathbf{Y}}^{\mathbf{q}}_{i3} \bar{u}_L^i t_R + \tilde{\mathbf{Y}}^{\mathbf{q}}_{3i} \bar{t}_L u_R^i \right) + \text{h.c.} \right], \quad (3)$$

with $i = 1, 2$.

The decay widths read respectively:

$$\Gamma(t \rightarrow q^i S) = \frac{v^2}{64\pi\Lambda^2} \left[(\mathbf{Y}^{\mathbf{q}}_{i3})^2 + (\mathbf{Y}^{\mathbf{q}}_{3i})^2 \right] m_t (1 - x^2)^2, \quad (4)$$

$$\begin{aligned} \Gamma(t \rightarrow q^i SS) = & \frac{v^2}{512\pi^3\Lambda^4} \left[(\tilde{\mathbf{Y}}^{\mathbf{q}}_{i3})^2 + (\tilde{\mathbf{Y}}^{\mathbf{q}}_{3i})^2 \right] m_t^3 \left[\frac{1}{3} \sqrt{1 - 4x^2} (1 + 5x^2 - 6x^4) \right. \\ & \left. + 2(x^2 - 2x^4 + 2x^6) \log \frac{2x^2}{1 - 2x^2 + \sqrt{1 - 4x^2}} \right], \end{aligned} \quad (5)$$

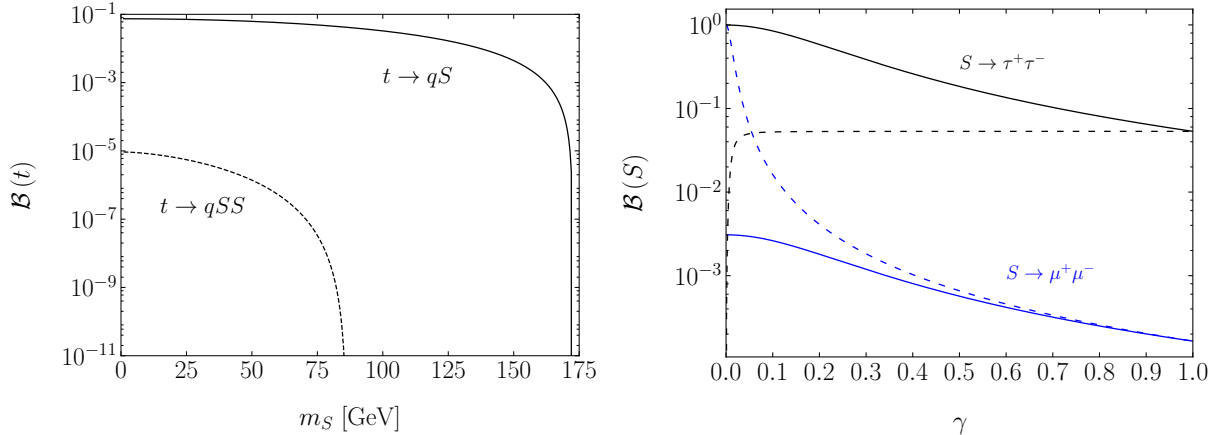


Figure 1: *Left)* Top branching ratios as a function of the mass of S , for $\tilde{\mathbf{Y}}_{i3}^q = \tilde{\mathbf{Y}}_{3i}^q = \mathbf{Y}_{i3}^q = \mathbf{Y}_{3i}^q = 1$ and $\Lambda = 1$ TeV. *Right)* Scalar branching ratios into muons (blue) and taus (black), as a function of the \mathbb{Z}_2 breaking parameter, γ , for $m_S = 100$ GeV. We represent two cases: (in solid lines) $\gamma_\ell = \gamma_\tau = 1$ while $\gamma_q = \gamma$; and (in dashed lines) $\gamma_\ell = 1$ and $\gamma_\tau = \gamma_q = \gamma$.

where we have defined $x = m_S/m_t$. Taking $\Gamma_t \sim 1.4$ GeV as reference value of the top width [42], we show in the left panel of Fig. 1 the branching ratio of the top quark into Sq and SSq for $\tilde{\mathbf{Y}}_{i3}^q = \tilde{\mathbf{Y}}_{3i}^q = \mathbf{Y}_{i3}^q = \mathbf{Y}_{3i}^q = 1$ and $\Lambda = 1$ TeV for different values of m_S .

The scalar S can subsequently decay into fermions. In this article we focus on the channel $S \rightarrow \ell^+\ell^-$. Assuming that this decay mode dominates the S width while $t \rightarrow q^i S$ requires that only \mathbf{Y}_{i3}^q (and/or \mathbf{Y}_{3i}^q) and \mathbf{Y}_{jj}^f , $j = 1, 2, 3$, are non vanishing. This scenario does not easily arise in UV models, where diagonal couplings of S to quarks are generally also present, proportional to masses, and $b\bar{b}$ dominates the S width; also due to the larger number of colours with respect to leptons [28]. Still, the branching ratio to taus is only an order of magnitude smaller. Thus, we will consider this unexplored S decay in the context of top FCNCs in this paper. For its cleanness, we will also consider the dimuon channel.

Prospects are very different if $t \rightarrow q^i SS$ instead. From the theory point of view, it can well be that a \mathbb{Z}_2 symmetry $S \rightarrow -S$ is only (or mostly) broken in the lepton sector. Or even just in the muon and electron side; in which case the dilepton decay of S is dominant. Let us write $\mathbf{Y}_{jj}^f = \gamma_{f_j} y_{f_j}$, where y_{f_j} is the fermion Yukawa and $0 < \gamma_{f_j} < 1$ parameterizes the degree of breaking of the \mathbb{Z}_2 . In the right panel of Fig. 1 we show the branching ratio of S into taus and muons for different assumptions on this parameter.

The interactions above arise very naturally within CHMs [43,44], where both the Higgs and S are pseudo-Goldstone bosons associated with the spontaneous global symmetry breaking \mathcal{G}/\mathcal{H} driven in a new strong sector at the confinement scale $\Lambda \sim$ TeV. In these models, the global symmetry is only approximate; being explicitly broken by the linear mixing between the elementary SM fermions and composite operators. (Or equivalently, by embedding the SM fermions in incomplete multiplets of \mathcal{G} .)

As a matter of example, let us consider the next-to-minimal CHM based on the coset

$SO(6)/SO(5)$ [3]. The generators of $SO(6)$ can be split into $SO(5)$ generators, T , and coset generators, X :

$$T_{ij}^{mn} = -\frac{i}{\sqrt{2}}(\delta_i^m \delta_j^n - \delta_i^n \delta_j^m) \quad X_{ij}^{mn} = -\frac{i}{\sqrt{2}}(\delta_i^m \delta_j^6 - \delta_i^6 \delta_j^m), \quad (6)$$

with $m < n \in [1, 5]$. The pNGB matrix reads

$$U = \begin{bmatrix} \mathbf{1}_{3 \times 3} & & & & & \\ & 1 - h^2/(\Lambda^2 + \Pi) & -hS/(\Lambda^2 + \Pi) & h/\Lambda & & \\ & -hS/(\Lambda^2 + \Pi) & 1 - S^2/(\Lambda^2 + \Pi) & S/\Lambda & & \\ & -h/\Lambda & -S/\Lambda & \Pi/\Lambda^2 & & \\ & & & & & \end{bmatrix}, \quad \Pi = \Lambda^2 \left(1 - \frac{h^2}{\Lambda^2} - \frac{S^2}{\Lambda^2} \right)^{1/2}. \quad (7)$$

Let us consider the regime in which the LH quarks are embedded in the representation **6**, while RH up quarks do in both the **6** and the **15**. Explicitly:

$$Q_L^I = \frac{1}{\sqrt{2}}(id_L^I, d_L^I, iu_L^I, -u_L^I, 0, 0), \quad U_{R_1}^I = (0, 0, 0, 0, i\gamma_q u_R^I, u_R^I) \quad (8)$$

$$\text{and} \quad U_{R_2}^I = i(T^{12} - T^{34})u_R^I, \quad (9)$$

with I running over the three quark families and γ_q a positive number. To zero momentum and two fermions, only two invariants can be built upon the spurions above. One arises from the product of the singlets in the decompositions $\mathbf{6}_{Q_L, U_{R_1}} = \mathbf{1} + \mathbf{5}$. The second one results from the scalar product of the fiveplets in the decompositions $\mathbf{6}_{Q_L} = \mathbf{1} + \mathbf{5}$ and $\mathbf{15}_{U_{R_2}} = \mathbf{5} + \mathbf{10}$. Mathematically:

$$L = \Lambda y_{IJ}^{(1)} (\overline{U^T Q_L^I})_6 (U^T U_{R_1}^J)_6 - \Lambda y_{IJ}^{(2)} (\overline{U^T Q_L^I})_m (\text{Tr}[U^T U_{R_2}^J U X^{m6}]) \quad (10)$$

$$= \frac{1}{\sqrt{2}} \overline{u_L^I} h u_R^J \left[y_{IJ}^{(1)} \left(-1 + i\gamma \frac{S}{\Lambda} + \frac{h^2}{2\Lambda^2} + \frac{S^2}{2\Lambda^2} \right) + y_{IJ}^{(2)} + \dots \right] + \text{h.c.}, \quad (11)$$

with the ellipsis representing terms suppressed by further powers of $1/\Lambda$. Comparing the two equations above with Eq. 3, we find that $\mathbf{Y}^{\mathbf{q}}_{ij} \sim \gamma y_{ij}^{(1)}$ and $\tilde{\mathbf{Y}}^{\mathbf{q}}_{ij} \sim y_{ij}^{(1)}$. Thus, in general, these matrices are not aligned with the Yukawa matrix $\sim y^{(1)} - y^{(2)}$ and therefore introduce FCNCs.

If the leptons are only embedded in six-dimensional representations we obtain, upon rotation:

$$L = -\frac{y_l^I}{\sqrt{2}} \overline{l_L^I} h e_R^I \left[1 - \gamma_l \frac{S}{\Lambda} + \dots \right] + \text{h.c.} \quad (12)$$

The assumption that leptons mix with only one representation of the composite sector implies that FCNCs vanish; $\mathbf{Y}^{\mathbf{l}}$ is automatically diagonal in the physical basis. In fact it is proportional to the lepton Yukawa matrix. Thus, the S decay to taus is expected to dominate. $S \rightarrow \mu^+ \mu^-$ should not be neglected, though. First, because $m_\mu/m_\tau \sim 0.06$ is not dramatically small. And second because if taus couple only to the **15**, or γ_τ is small, then the muon channel dominates the S width; we refer again to Fig. 1.

We also note that, within the class of CHMs we have just described, there are also Higgs mediated FCNCs. Searches for these have been performed in *e.g.* Refs. [32, 33]. However, as it was first pointed out in Ref. [28], exploring S mediated FCNCs is much more promising for several reasons: (i) they arise at dimension five, and therefore are less suppressed by powers of v/Λ ; (ii) the mass of S can lie at values where the SM background is less prominent; and (iii) contrary to what occurs in the case of S , there is no parameter space in which the Higgs boson can decay sizably into the cleanest final states such as $\mu^+\mu^-$.

Currently, only a few experimental searches are (marginally) sensitive to the interactions discussed before. The first one is the ATLAS search for $t \rightarrow Zq$ of Ref. [45]. In the control region dubbed CR1, this analysis requires three light leptons (either electrons or muons, denoted by ℓ), two of them of the same flavour and opposite sign (SFOS), exactly one b -tagged jet and at least two more light jets. Most importantly, the two SFOS leptons with invariant mass closer to the Z mass ~ 91.2 GeV are required to be within a 15 GeV mass window around the Z pole. Consequently $t \rightarrow Sq$ events with $m_S \neq m_Z$ are captured in this region.

The possibility of using this control region to constrain interactions not necessarily leading to $t \rightarrow Zq$ was first pointed out in Ref. [34], which also reports the maximum number of signal events allowed by the analysis to be $s_{\max} = 143$. In order to estimate the LHC sensitivity to the proposed signal, we rely on home-made routines based on ROOT v6 [46] with FastJet v3 [47]. The simulated events were generated with MadGraph v5 [48] and Pythia v8 [49]. For the efficiency for selecting $t\bar{t}$ events in the semileptonic channel we obtain $\epsilon \sim 0.2$. The expected number of signal events at $\mathcal{L} = 36 \text{ fb}^{-1}$ reads therefore

$$N \sim 2 \times \sigma(pp \rightarrow t\bar{t}) \times \mathcal{B}(t \rightarrow \ell^+ \nu b) \times \mathcal{B}(t \rightarrow Sq, S \rightarrow \ell^+ \ell^-) \times \mathcal{L} \times \epsilon, \quad (13)$$

with $\mathcal{B}(t \rightarrow \ell^+ \nu b) \sim 0.27$ [42] and $\sigma(pp \rightarrow t\bar{t}) = 832 \pm 29 \text{ pb}$ at 13 TeV [50]. This implies that the upper limit on $\mathcal{B}(t \rightarrow Sq, S \rightarrow \ell^+ \ell^-)$ is $\sim 143/(3 \times 10^6) \sim 5 \times 10^{-5}$. This bound in turn translates to a bound on $(\mathbf{Y}^{\mathbf{q}_{i3}})^2 + (\mathbf{Y}^{\mathbf{q}_{3i}})^2 \lesssim 10^{-4} (\Lambda/v)^2$, (for $m_S \sim m_t/2$). To the best of our knowledge there are no relevant constraints on the tau channel.

Another analysis sensitive to the proposed top interactions is the ATLAS search for SUSY in multilepton final states [51]. The maximum number of allowed signal events in this analysis for $L = 150 \text{ fb}^{-1}$ is larger than 20. Upon implementing only a few of the cuts, we have checked that such big number arises within our framework only if FCNC couplings are larger than 1 for $\Lambda = 1 \text{ TeV}$. It will become clear in the following sections that the dedicated analyses we propose are sensitive to a much larger region of the parameter space.

Other similar searches suffer from the same problem. Namely, they are too broad in scope and therefore the background is large enough to hide the signal we are interested in. Consequently, dedicated searches are required and we discuss three examples in very detail in the subsequent sections, aiming to explore $pp \rightarrow tS + j, S \rightarrow \mu^+\mu^-$, $pp \rightarrow tS + j, S \rightarrow \tau^+\tau^-$ and $pp \rightarrow tSS + j, S \rightarrow \mu^+\mu^-$. Note hence that the top FCNCs can be either in the decay of the top quark when is pair-produced via QCD (with the extra jet from radiation), or directly in the core of tS associate production.

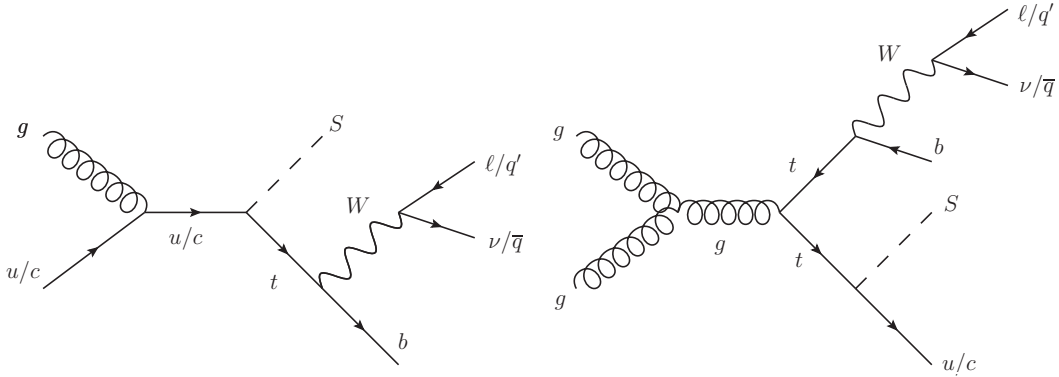


Figure 2: Representative Feynman diagrams for the production of a single top quark in association with S via an FCNC interaction (left) and for the top-quark pair production with an FCNC top-quark decay into the extra singlet (right).

In light of the discussion above, we assume hereafter that $\Lambda \gtrsim \text{TeV}$ and all Wilson coefficients vanish with the exception of ${}^2 \mathbf{Y}_{22}^1$ (or \mathbf{Y}_{33}^l) and either \mathbf{Y}_{13}^q or \mathbf{Y}_{23}^q or $\tilde{\mathbf{Y}}_{13}^q$ (depending on which process we study). We quantify the results in terms of seven benchmark masses: $m_S = 20, 50, 80, 90, 100, 120$ and 150 GeV. Given the reduced phase space for $t \rightarrow SSq$, we include in addition the benchmark masses $m_S = 30, 40, 60$ and 70 GeV in the analysis for this channel. The reach of the dedicated analyses proposed below will be compared to the following Benchmark Points (BP):

$$\begin{aligned}
 \text{BP 1: } & \mathbf{Y}_{i3}^q = \mathbf{Y}_{3i}^q = 0.01, \quad \Lambda = 5 \text{ TeV} \implies \mathcal{B}(t \rightarrow Sq) \sim 10^{-8} - 10^{-7}, \\
 \text{BP 2: } & \mathbf{Y}_{i3}^q = \mathbf{Y}_{3i}^q = 0.10, \quad \Lambda = 5 \text{ TeV} \implies \mathcal{B}(t \rightarrow Sq) \sim 10^{-6} - 10^{-5}, \\
 \text{BP 3: } & \mathbf{Y}_{i3}^q = \mathbf{Y}_{3i}^q = 0.10, \quad \Lambda = 1 \text{ TeV} \implies \mathcal{B}(t \rightarrow Sq) \sim 10^{-4} - 10^{-3}, \\
 \text{BP 4: } & \tilde{\mathbf{Y}}_{i3}^q = \tilde{\mathbf{Y}}_{3i}^q = 1.00, \quad \Lambda = 5 \text{ TeV} \implies \mathcal{B}(t \rightarrow SSq) \sim 10^{-11} - 10^{-8}, \\
 \text{BP 5: } & \tilde{\mathbf{Y}}_{i3}^q = \tilde{\mathbf{Y}}_{3i}^q = 0.20, \quad \Lambda = 1 \text{ TeV} \implies \mathcal{B}(t \rightarrow SSq) \sim 10^{-10} - 10^{-7}, \\
 \text{BP 6: } & \tilde{\mathbf{Y}}_{i3}^q = \tilde{\mathbf{Y}}_{3i}^q = 1.00, \quad \Lambda = 1 \text{ TeV} \implies \mathcal{B}(t \rightarrow SSq) \sim 10^{-8} - 10^{-5}, \quad (14)
 \end{aligned}$$

with $i = 1, 2$. The range in the branching ratio ensues from the range of values of m_S .

3 Search for $t \rightarrow Sq, S \rightarrow \mu^+ \mu^-$

The singlet S can arise either in the production or in the decay of the top quark; see the diagrams on figure 2. This leads to a final state with exactly one S , one top quark decaying into Wb and eventually an additional light quark $q = u, c$. In this first analysis we study the scenario where S decays into a pair of muons. We focus on the leptonic decay of the W . Hence, at the detector level, we expect three charged leptons, several jets (at least one originated by a b meson) and significant missing energy.

²Note that for $10 \text{ GeV} < m_S < 100 \text{ GeV}$ current data from ATLAS, CMS and BaBar only constrain $\mathbf{Y}^1 \gtrsim 0.1$ [22] for $\Lambda = 1 \text{ TeV}$. Even for much smaller values, S decays promptly.

We generate signal and background events at $\sqrt{s} = 13$ TeV with `MadGraph v5` [48], with signal model being implemented in `Feynrules v2` [52]. We subsequently use `Pythia v8` [49] for simulating the initial and final state radiation, the parton shower and the hadronization. At parton level, only leptons and photons with a transverse momentum higher than 10 GeV are considered. For the jets, this cut rises to 20 GeV. Concerning the absolute pseudo-rapidity $|\eta|$, jets can have a value of this variable lower than 5 while for leptons and photons it should be lower than 2.5.

We use the Parton Distribution Functions `NNPDF23LO` [53] and set the renormalization and factorization scales to the default dynamical `MadGraph` value. The total background comprises samples from tW , $t\bar{t}V$, VV , ZVV , $t\bar{t}$, $V + \text{jets}$ and tZ , with $V = W, Z$. For the present analysis, the most dominant background comes from tZ and $t\bar{t}$ production, where $t \rightarrow Wb$ and all gauge bosons are assumed to decay into muons. Such exclusive samples are motivated by the targeted trilepton final state of the signal. (Although the tW , diboson and $Z + \text{jets}$ processes have the largest cross sections, they become irrelevant after the cuts on the number of reconstructed leptons and jets; check Tab. 3.)

We use `Delphes` [54] to simulate the detector effects with the default CMS detector card. An electron (muon) is considered to be isolated if the sum of the transverse momenta of all particles above $p_T^{\text{min}} = 0.5$ GeV that lie within a cone of radius $R = 0.5$, normalized to the lepton p_T , is smaller than 0.12 (0.25).

Jets are defined using the anti- k_t algorithm [55] with a radius parameter of $R = 0.5$. All the jets are required to have $p_T > 25$ GeV and to lie within a pseudorapidity range of $|\eta| < 2.5$. Leptons must have $p_T > 15$ GeV and $|\eta| < 2.4$ (2.5) for muons (electrons); the hardest lepton is also required to have $p_T > 25$ GeV. The effect of the previous requirements on the transverse momentum and pseudorapidity of jets and leptons can be found in the yields tables, labeled “basic cuts”.

We select events with exactly three isolated leptons and at least one jet, one of them required to be tagged as a b -quark. The `Delphes` CMS card was used to parameterize the p_T dependent tagging efficiencies for jets initiated by b -quarks, as well as to take into account the mistag probability. As an example, for a b -jet with a transverse momentum of 30 GeV, the tagging efficiency is 55% and the mistag rate for a c -jet with the same p_T is 12%. The scalar resonance, S , is reconstructed from the hardest $\mu^+\mu^-$ pair (if there is none, the event is discarded). The longitudinal component of the missing neutrino four-momentum (p_ν) is reconstructed by demanding $m_W^2 = (p_\ell + p_\nu)^2$, where p_ℓ is the four-momentum of the lepton not coming from the scalar decay and $m_W = 81.2$ GeV is our reference value for the W boson mass. Among the two possible solutions, we use the one with smaller absolute value.

Both p_ν and p_ℓ are then added to the four-momentum of the b -jet to reconstruct the SM top quark; its invariant mass being dubbed m_t^{rec} . We show the distributions of the scalar and top reconstructed masses for two signal benchmark points and for the relevant background components in Fig. 3. The label EXC manifests that the corresponding backgrounds are generated assuming the exclusive leptonic mode. We require the $m_{t,\text{rec}}$ variable to be within a window of 50 GeV from the reference top mass $m_t = 172.5$ GeV. We impose an additional cut of 1 TeV on maximum invariant mass of the total system, m_{total} , in order to stay in the regime of validity of the effective field theory. The impact on

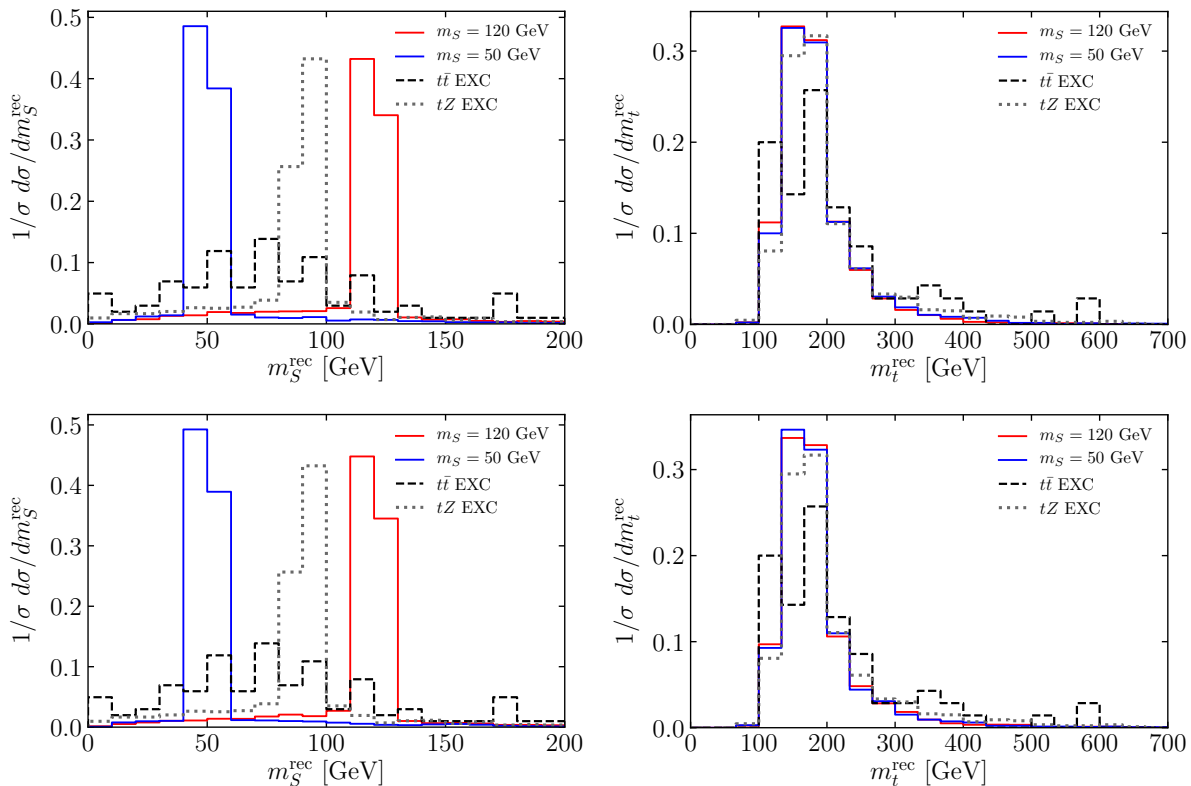


Figure 3: The reconstructed scalar (left) and top (right) mass in the analysis proposed for $t \rightarrow Sq$, $S \rightarrow \mu^+\mu^-$. In the upper (bottom) panel, $q = c$ (u). We represent the distributions of two signal benchmark points and the two major background components, after the cut on the particle multiplicities; the background samples are generated exclusively, *i.e.* only gauge bosons decays into muons are included. The distributions assume a collected luminosity of $\mathcal{L} = 150 \text{ fb}^{-1}$.

the expected signal yield caused by this additional requirement is minor when compared to the other selection cuts, and increases for higher masses (varying between 1.5% and 7% for masses of the scalar of 20 GeV and 150 GeV, respectively). The final cut requires the scalar S candidate invariant mass, m_S^{rec} , to be within a mass window of ± 30 GeV around the probed value of m_S .

The cut flow for the signal with an up and with a charm quark is given in Tabs. 1 and 2, respectively. The scalar mass-independent yields for the background components are shown in Tab. 3 while the mass-dependent one is given in Tab. 4. An integrated luminosity of 150 fb^{-1} is considered for this analysis.

Upper limits on the signal cross section are obtained under the signal absence hypothesis, using the CL_s method [56]. For this, the distribution of the invariant mass of the reconstructed scalar S after all selection cuts is fitted with **OpTHyLic** [57]. A total of 20 bins per signal point are considered and Poissonian statistical uncertainties on each bin of the distributions are included in the computation. An expected upper limit on the signal strength, $\sigma_{95\%}/\sigma_{\text{th}}$ ($pp \rightarrow tS(q)$, $S \rightarrow \mu^+\mu^-$) at 95% confidence level (CL) is then

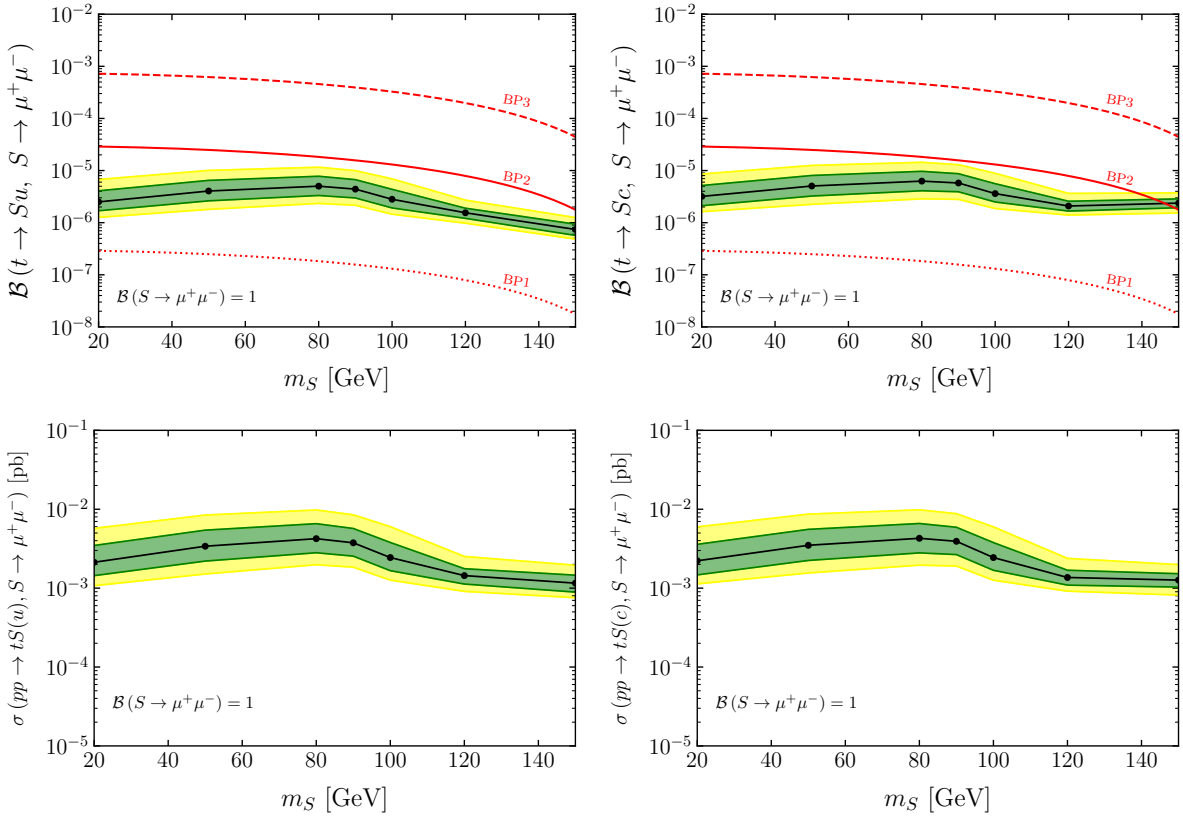


Figure 4: In the upper (bottom) panels, we show the 95% CL limits on the branching ratio (cross section times branching ratio) that can be tested in the $\mu^+\mu^-$ channel, in the analysis proposed for $t \rightarrow Sq$, $S \rightarrow \mu^+\mu^-$, with $q = u$ (c) in the panels on the left (right). The limits are obtained for a collected luminosity $\mathcal{L} = 150 \text{ fb}^{-1}$. The green and yellow bands show the $\pm 1\sigma$ and $\pm 2\sigma$ uncertainty on the limits, respectively. Superimposed are the theoretical expectations in three BPs.

obtained. The signal cross section, σ_{th} is computed with **MadGraph v5**. The ± 1 and $\pm 2\sigma$ variations are also computed, taking into account the statistical uncertainty arising from finite Monte Carlo samples.

We present the results in Fig. 4, where we show the 95% CL upper limits on the top branching ratio $\mathcal{B}(t \rightarrow Sq, S \rightarrow \mu^+\mu^-)$ and cross section $\sigma(pp \rightarrow tS(q), S \rightarrow \mu^+\mu^-)$. The ± 1 and $\pm 2\sigma$ bands are plotted in green and yellow, respectively.

Note that the sensitivity worsens at $m_S \sim m_Z$ due to larger impact of the backgrounds with Z -bosons. This effect, however, is attenuated by two factors: (i) the mass window around the singlet mass in which the events are selected is relatively large; and (ii) while the tZ background distribution is larger around 90 GeV, the combination of the tZ and $t\bar{t}$ background components is equally important in the neighboring bins of the reconstructed scalar mass distribution.

Cuts/ m_S	20 GeV	50 GeV	80 GeV	90 GeV	100 GeV	120 GeV	150 GeV
Basic cuts	29445 \pm 133	25065 \pm 113	18525 \pm 84	16095 \pm 73	13623 \pm 62	8829 \pm 40	3306 \pm 15
$n_\ell = 3$	6092 \pm 61	5597 \pm 54	4769 \pm 43	4295 \pm 38	3642 \pm 32	2416 \pm 21	899 \pm 8
$n_j > 1$	6033 \pm 60	5537 \pm 53	4708 \pm 42	4249 \pm 37	3589 \pm 32	2378 \pm 21	865 \pm 8
$n_b = 1$	3249 \pm 44	2961 \pm 39	2543 \pm 31	2301 \pm 27	1914 \pm 23	1265 \pm 15	479 \pm 6
$n_{\mu^+\mu^-} = 1$	3247 \pm 44	2959 \pm 39	2542 \pm 31	2300 \pm 27	1913 \pm 23	1265 \pm 15	478 \pm 6
$ m_t^{\text{rec}} - m_t < 50 \text{ GeV}$	2763 \pm 41	2507 \pm 36	2152 \pm 29	1961 \pm 25	1625 \pm 21	1075 \pm 14	403 \pm 5
$m_{\text{total}} < 1 \text{ TeV}$	2713 \pm 40	2468 \pm 36	2089 \pm 28	1893 \pm 25	1556 \pm 21	1013 \pm 13	375 \pm 5
$ m_S^{\text{rec}} - m_S < 30 \text{ GeV}$	1908 \pm 34	1729 \pm 30	1440 \pm 23	1297 \pm 21	1062 \pm 17	690 \pm 11	252 \pm 4

Table 1: Event yields after each cut for the seven benchmark signal points, in the analysis for $t \rightarrow Su, S \rightarrow \mu^+\mu^-$. We fix $Y_{13} = Y_{31} = 0.1, \Lambda = 1 \text{ TeV}$ and $\mathcal{B}(S \rightarrow \mu^+\mu^-) = 1$. The event yields presented assume a collected luminosity of $\mathcal{L} = 150 \text{ fb}^{-1}$.

Cuts/ m_S	20 GeV	50 GeV	80 GeV	90 GeV	100 GeV	120 GeV	150 GeV
Basic cuts	24120 \pm 109	20655 \pm 93	14985 \pm 68	12825 \pm 58	10597 \pm 48	6204 \pm 28	1127 \pm 5
$n_\ell = 3$	5235 \pm 51	4923 \pm 46	4070 \pm 35	3633 \pm 31	3050 \pm 26	1836 \pm 15	362 \pm 3
$n_j > 1$	5214 \pm 51	4906 \pm 46	4050 \pm 35	3616 \pm 31	3030 \pm 26	1821 \pm 15	352 \pm 3
$n_b = 1$	2705 \pm 37	2520 \pm 33	2103 \pm 25	1870 \pm 22	1571 \pm 18	957 \pm 11	188 \pm 2
$n_{\mu^+\mu^-} = 1$	2705 \pm 37	2520 \pm 33	2102 \pm 25	1870 \pm 22	1571 \pm 18	957 \pm 11	188 \pm 2
$ m_t^{\text{rec}} - m_t < 50 \text{ GeV}$	2229 \pm 33	2072 \pm 30	1754 \pm 23	1551 \pm 20	1311 \pm 17	801 \pm 10	161 \pm 2
$m_{\text{total}} < 1 \text{ TeV}$	2194 \pm 33	2038 \pm 29	1708 \pm 23	1488 \pm 20	1248 \pm 16	749 \pm 10	148 \pm 2
$ m_S^{\text{rec}} - m_S < 30 \text{ GeV}$	1502 \pm 28	1406 \pm 24	1166 \pm 19	1003 \pm 16	829 \pm 13	497 \pm 8	100 \pm 2

Table 2: Event yields after each cut for the seven benchmark signal points, in the analysis for $t \rightarrow Sc, S \rightarrow \mu^+\mu^-$. We fix $Y_{23} = Y_{32} = 0.1, \Lambda = 1 \text{ TeV}$ and $\mathcal{B}(S \rightarrow \mu^+\mu^-) = 1$. The event yields presented assume a collected luminosity of $\mathcal{L} = 150 \text{ fb}^{-1}$.

Cuts/Background	tW	$t\bar{W}/t\bar{t}Z$	ZZZ/WWZ	$ZZ/WZ/WW$	$t\bar{t}$	tZ
Basic cuts	8352000 \pm 37351	934 \pm 9	1385 \pm 6	14835000 \pm 66344	852600 \pm 1206	1724 \pm 8
$n_\ell = 3$	334 \pm 236	5.2 \pm 0.7	10.1 \pm 0.5	16615 \pm 2220	348 \pm 24	128 \pm 2
$n_j > 1$	334 \pm 236	5.2 \pm 0.7	9.1 \pm 0.5	8011 \pm 1542	326 \pm 24	128 \pm 2
$n_b = 1$	334 \pm 236	2.2 \pm 0.5	1.0 \pm 0.2	< 74	172 \pm 17	65 \pm 1
$n_{\mu^+\mu^-} = 1$	< 42	1.1 \pm 0.3	0.7 \pm 0.1	—	172 \pm 17	39 \pm 1
$ m_t^{\text{rec}} - m_t < 50 \text{ GeV}$	—	0.7 \pm 0.3	0.4 \pm 0.1	—	114 \pm 14	31 \pm 1
$m_{\text{total}} < 1 \text{ TeV}$	—	0.3 \pm 0.2	0.25 \pm 0.08	—	80 \pm 12	23.2 \pm 0.9

Table 3: Event yields after each cut for the dominant backgrounds, in the analysis for $t \rightarrow Sq, S \rightarrow \mu^+\mu^-$. The $Z + \text{jets}$ sample is reduced to negligible values after the cut on the lepton multiplicity. The event yields presented assume a collected luminosity of $\mathcal{L} = 150 \text{ fb}^{-1}$.

Background/ m_S	20 GeV	50 GeV	80 GeV	90 GeV	100 GeV	120 GeV	150 GeV
$t\bar{t}W/t\bar{t}Z$	< 0.09	< 0.09	0.2 ± 0.1	0.2 ± 0.1	0.2 ± 0.1	0.2 ± 0.1	< 0.09
ZZZ/WWZ	0 ± 0	0.06 ± 0.04	0.22 ± 0.08	0.17 ± 0.07	0.17 ± 0.07	< 0.03	< 0.03
$t\bar{t} (\mu)$	12 ± 4	34 ± 8	39 ± 8	39 ± 8	36 ± 8	15 ± 5	3 ± 2
tZ	1.8 ± 0.2	3.3 ± 0.3	18.6 ± 0.8	18.4 ± 0.8	17.9 ± 0.8	11.4 ± 0.6	0.8 ± 0.2

Table 4: Event yields for the last selection cut on m_S^{rec} for the dominant backgrounds, in the analysis for $t \rightarrow Sq, S \rightarrow \mu^+\mu^-$.

4 Search for $t \rightarrow Sq, S \rightarrow \tau^+\tau^-$

We focus now on the scenario where the scalar S decays to a pair of taus, concentrating on the hadronic decays of the latter. Again, we focus on the leptonic decay of the W . Thus, we require events to contain exactly one light lepton and at least three jets, from which exactly one must be b -tagged and exactly two must be tagged as taus decaying into hadrons. The efficiency for τ -tagging is 60% while the misidentification rate is 1% with no dependency on the transverse momentum. Jets and leptons are defined in the same p_T and $|\eta|$ ranges as in the previous analysis.

The dominant backgrounds for this channel are the exclusive tW and $t\bar{t}$ processes, where the top quark is assumed to decay to Wb and $W \rightarrow \tau\nu$. Indeed, after the aforementioned cuts on the particle multiplicities, the other background components (with the largest cross sections) become irrelevant; see Tab. 7.

We (partially) reconstruct the scalar S from the two tau-jets obtaining its invariant mass, m_S^{rec} . In the left panels of Fig. 5 we show the normalized distribution of this variable, after the basic selection cuts, in two signal BPs and in the main backgrounds. In the same figure, we plot the transverse mass distribution of the system composed by the lepton, the b -tagged jet, the reconstructed scalar and the missing energy. We require this later variable to be smaller than 500 GeV. Finally, events are required to fulfill $|m_S - m_S^{\text{rec}}| < 30$ GeV, where m_S^{rec} is the mas of the reconstructed scalar candidate and m_S is the corresponding value being probed.

The cut flows for the signal in the up quark and in the charm quark cases are given in Tabs. 5 and 6; respectively. Likewise, Tab. 7 shows the m_S -independent yields for the different backgrounds and in Tab. 8 we write the mass-dependent ones. Similarly to the previous analysis, the expected upper limit on the signal strength, $\sigma_{95\%}/\sigma_{\text{th}}(pp \rightarrow tS(q), S \rightarrow \tau^+\tau^-)$, is obtained using the invariant mass of the scalar S candidate distributed into 20 bins. The 95% CL upper limits on the branching ratio $\mathcal{B}(t \rightarrow Sq, S \rightarrow \tau^+\tau^-)$ and on the cross section $\sigma(pp \rightarrow tS(q), S \rightarrow \tau^+\tau^-)$ are shown in Fig. 6.

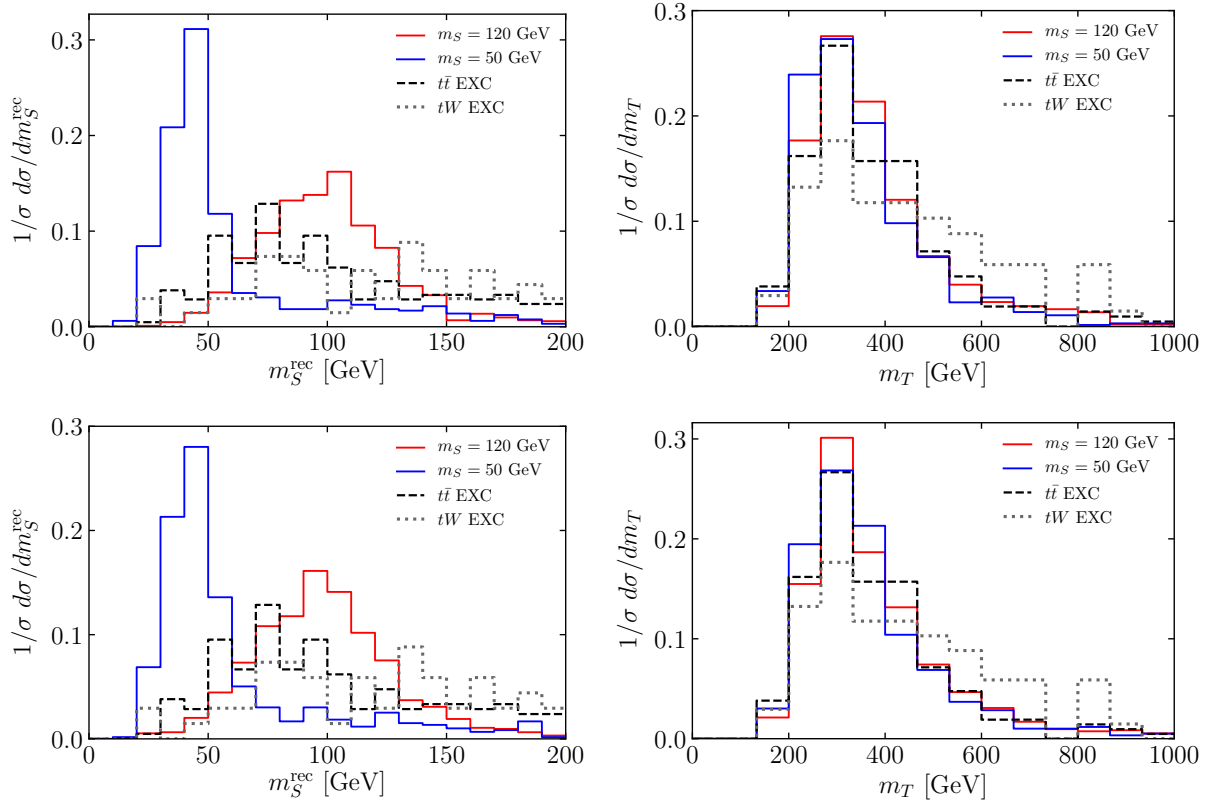


Figure 5: The reconstructed scalar mass (left) and the transverse mass of the system composed by the lepton, the b -jet, the reconstructed S and missing energy (right) in the analysis proposed for $t \rightarrow Sq$, $S \rightarrow \tau^+\tau^-$. In the upper (bottom) panel, $q = c$ (u). We represent the distributions of two signal benchmark points and the two major background components, after the cut on the particle multiplicities; the background samples are generated exclusively, *i.e.* only gauge bosons decays into taus are included. The distributions assume a collected luminosity of $\mathcal{L} = 150 \text{ fb}^{-1}$.

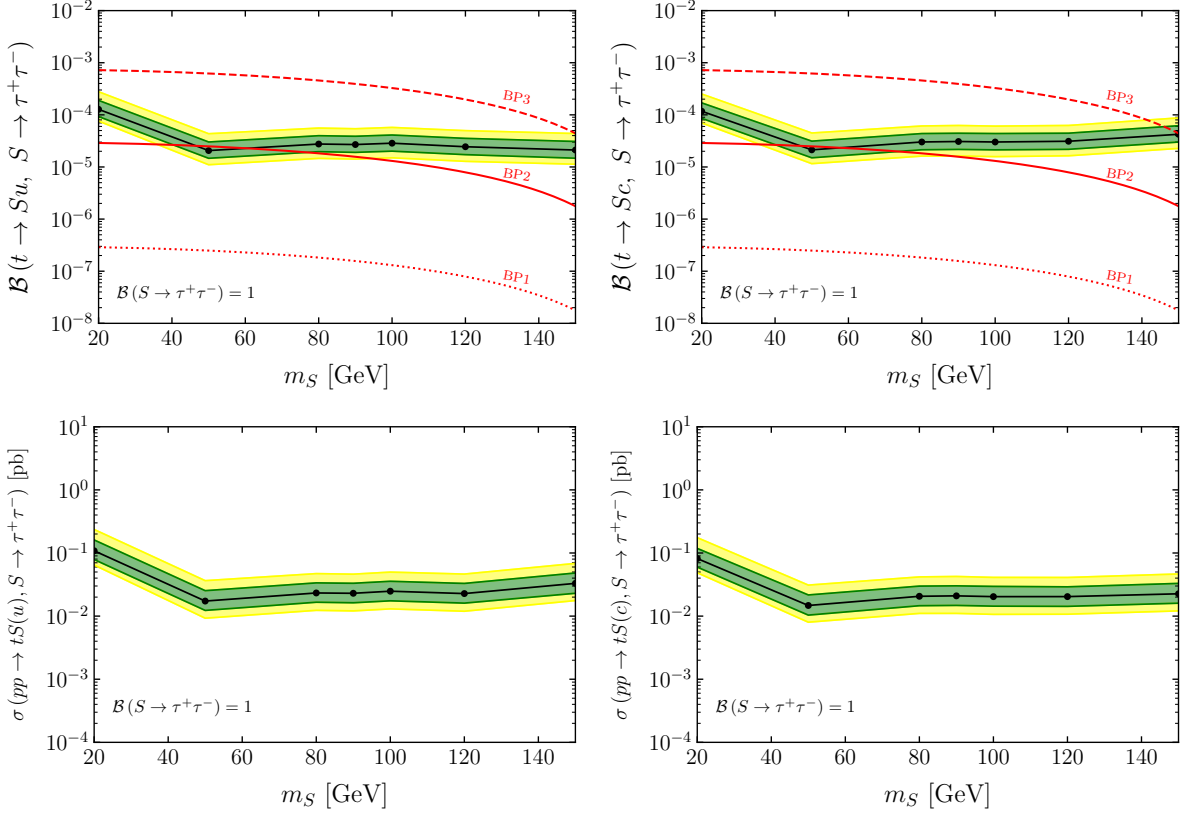


Figure 6: In the upper (bottom) panels, we show the 95% CL limits on the branching ratio (cross section times branching ratio) that can be tested in the $\tau^+\tau^-$ channel, in the analysis proposed for $t \rightarrow Sq$, $S \rightarrow \tau^+\tau^-$, with $q = u$ (c) in the panels on the left (right). The green and yellow bands show the $\pm 1\sigma$ and $\pm 2\sigma$ uncertainty on the limits, respectively. The limits are obtained for a collected luminosity $\mathcal{L} = 150 \text{ fb}^{-1}$. Superimposed are the theoretical expectations in three BPs.

Cuts/ m_S	20 GeV	50 GeV	80 GeV	90 GeV	100 GeV	120 GeV	150 GeV
Basic	29445 ± 133	25065 ± 113	18525 ± 84	16095 ± 73	13608 ± 62	8829 ± 40	3306 ± 15
$n_j > 3$	22290 ± 116	19293 ± 100	14509 ± 74	14698 ± 70	12432 ± 59	6864 ± 35	2439 ± 13
$n_b = 1$	12171 ± 86	10516 ± 73	7910 ± 55	12571 ± 64	10688 ± 55	3723 ± 26	1354 ± 10
$n_\ell = 1$	6148 ± 61	5251 ± 52	3975 ± 39	6804 ± 47	5814 ± 40	1826 ± 18	676 ± 7
$n_{\tau_h} = 2$	118 ± 8	306 ± 12	309 ± 11	3340 ± 33	2877 ± 28	171 ± 6	66 ± 2
$m_T < 500$ GeV	86 ± 7	259 ± 11	256 ± 910	280 ± 10	234 ± 8	143 ± 5	47 ± 2
$ m_S^{rec} - m_S < 30$ GeV	47 ± 5	220 ± 11	193 ± 9	236 ± 9	195 ± 7	79 ± 4	18 ± 1

Table 5: Event yields after each cut for the seven benchmark signal points, in the analysis for $t \rightarrow Su, S \rightarrow \tau^+ \tau^-$. We use $Y_{13} = Y_{31} = 0.1, \Lambda = 1$ TeV and $\mathcal{B}(S \rightarrow \tau^+ \tau^-) = 1$. The event yields presented assume a collected luminosity of $\mathcal{L} = 150 \text{ fb}^{-1}$.

Cuts/ m_S	20 GeV	50 GeV	80 GeV	90 GeV	100 GeV	120 GeV	150 GeV
Basic cuts	24120 ± 109	20655 ± 93	14985 ± 68	12816 ± 58	10597 ± 48	6204 ± 28	1127 ± 5
$n_j > 3$	19339 ± 98	16636 ± 84	12219 ± 61	11682 ± 55	8679 ± 43	5049 ± 25	873 ± 5
$n_b = 1$	10190 ± 71	8651 ± 60	6398 ± 44	10415 ± 52	4561 ± 31	2653 ± 18	465 ± 3
$n_\ell = 1$	5115 ± 50	4315 ± 43	3172 ± 31	5483 ± 38	2259 ± 22	1325 ± 13	233 ± 2
$n_{\tau_h} = 2$	107 ± 7	276 ± 11	256 ± 9	2730 ± 27	215 ± 7	131 ± 4	27.5 ± 0.8
$m_T < 500$ GeV	91 ± 7	243 ± 10	222 ± 8	244 ± 8	182 ± 6	111 ± 4	22.9 ± 0.7
$ m_S^{rec} - m_S < 30$ GeV	48 ± 5	203 ± 9	171 ± 7	207 ± 7	124 ± 5	62 ± 3	9.0 ± 0.5

Table 6: Event yields after each cut for the seven benchmark signal points, in the analysis for $t \rightarrow Sc, S \rightarrow \tau^+ \tau^-$. We fix $Y_{23} = Y_{32} = 0.1, \Lambda = 1$ TeV and $\mathcal{B}(S \rightarrow \tau^+ \tau^-) = 1$. The event yields presented assume a collected luminosity of $\mathcal{L} = 150 \text{ fb}^{-1}$.

Cuts/Background	$tW(\tau)$	$t\bar{W}/t\bar{t}Z$	ZZ/WWZ	$ZZ/WZ/WW$	$\bar{t}\bar{t}(\tau)$	tZ
Basic cuts	69715 ± 139	934 ± 9	1385 ± 6	14835000 ± 66344	111013 ± 165	1724 ± 8
$n_j > 3$	55080 ± 124	894 ± 9	1160 ± 6	8594806 ± 50498	89367 ± 148	1552 ± 7
$n_b = 1$	28047 ± 88	349 ± 6	264 ± 3	1333073 ± 19888	41365 ± 101	772 ± 5
$n_\ell = 1$	4460 ± 35	80 ± 3	44 ± 1	80406 ± 4884	5041 ± 35	282 ± 3
$n_{\tau_h} = 2$	19 ± 2	0.6 ± 0.2	0.05 ± 0.04	< 74	52 ± 4	0.4 ± 0.1
$m_T < 500$ GeV	11 ± 2	0.4 ± 0.2	0.05 ± 0.04	—	42 ± 3	0.3 ± 0.1

Table 7: Event yields after each cut for the dominant backgrounds, in the analysis for $t \rightarrow Sq, S \rightarrow \tau^+ \tau^-$. The $Z + \text{jets}$ sample is reduced to negligible values after the fifth cut. The event yields presented assume a collected luminosity of $\mathcal{L} = 150 \text{ fb}^{-1}$.

Background/ m_S	20 GeV	50 GeV	80 GeV	90 GeV	100 GeV	120 GeV	150 GeV
tW (τ)	0.6 ± 0.4	3.1 ± 0.9	5 ± 1	5 ± 1	5 ± 1	5 ± 1	4 ± 1
ttW/ttZ	< 0.09	< 0.09	0.3 ± 0.2	0.3 ± 0.2	0.2 ± 0.1	< 0.09	< 0.09
ZZZ/WWZ	< 0.03	< 0.03	< 0.03	< 0.03	< 0.03	< 0.03	< 0.03
$t\bar{t}$ (τ)	3.7 ± 0.9	17 ± 2	24 ± 2	21 ± 2	20 ± 2	14 ± 2	10 ± 1
tZ	< 0.03	0.07 ± 0.05	0.10 ± 0.06	0.10 ± 0.06	0.10 ± 0.06	0.10 ± 0.06	0.14 ± 0.07

Table 8: Event yields for the last selection cut on m_S^{rec} for the dominant backgrounds, in the analysis for $t \rightarrow Sq, S \rightarrow \tau^+\tau^-$. The event yields presented assume a collected luminosity of $\mathcal{L} = 150 \text{ fb}^{-1}$.

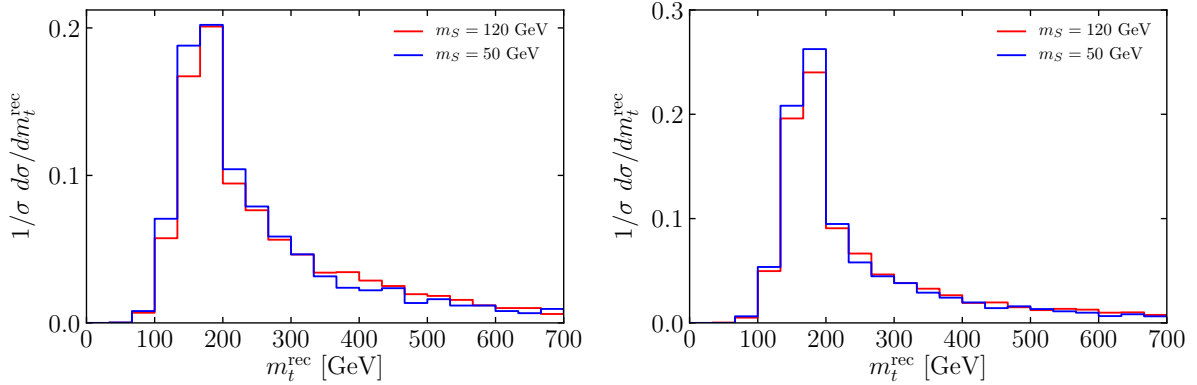


Figure 7: The reconstructed top mass in the analysis proposed for $t \rightarrow SSq, S \rightarrow \mu^+\mu^-$. In the left (right) panel, $q = c$ (u). The distributions assume a collected luminosity of $\mathcal{L} = 150 \text{ fb}^{-1}$.

5 Search for $t \rightarrow SSq, S \rightarrow \mu^+\mu^-$

Finally, let us develop an analysis to search for two singlet scalars produced in association with a top quark (or in the decay of a top quark in pair production), both decaying to a pair of muons. We focus on the hadronic decays of the W . The final state consists of four isolated leptons and at least three jets, one of them required to be b -tagged. Due to the large lepton multiplicity, all the background components are significantly reduced; with the additional cuts on the number of jets, most become negligible. We are left with six background events from the $t\bar{t}V$ and $t\bar{t}$ exclusive samples; see Tab. 11.

We reconstruct the top quark from a W boson and a b -jet; its invariant mass being m_t^{rec} . The W is reconstructed from the two light jets with invariant mass closest to m_W . We then require m_t^{rec} to be within a window of 50 GeV around the top mass. The two scalars S candidates are reconstructed by requiring two muons with opposite sign, with the event being rejected if no such candidates are found. The opposite-sign muons reconstructing the two scalars are those minimizing $|m_{S_1}^{\text{rec}} - m_{S_2}^{\text{rec}}|$, with $m_{S_{1,2}}^{\text{rec}}$ being the invariant mass of each pair of opposite sign muons. It is also required that the invariant mass of the total system, Sq , composed of the reconstructed top quark and the two scalars, is

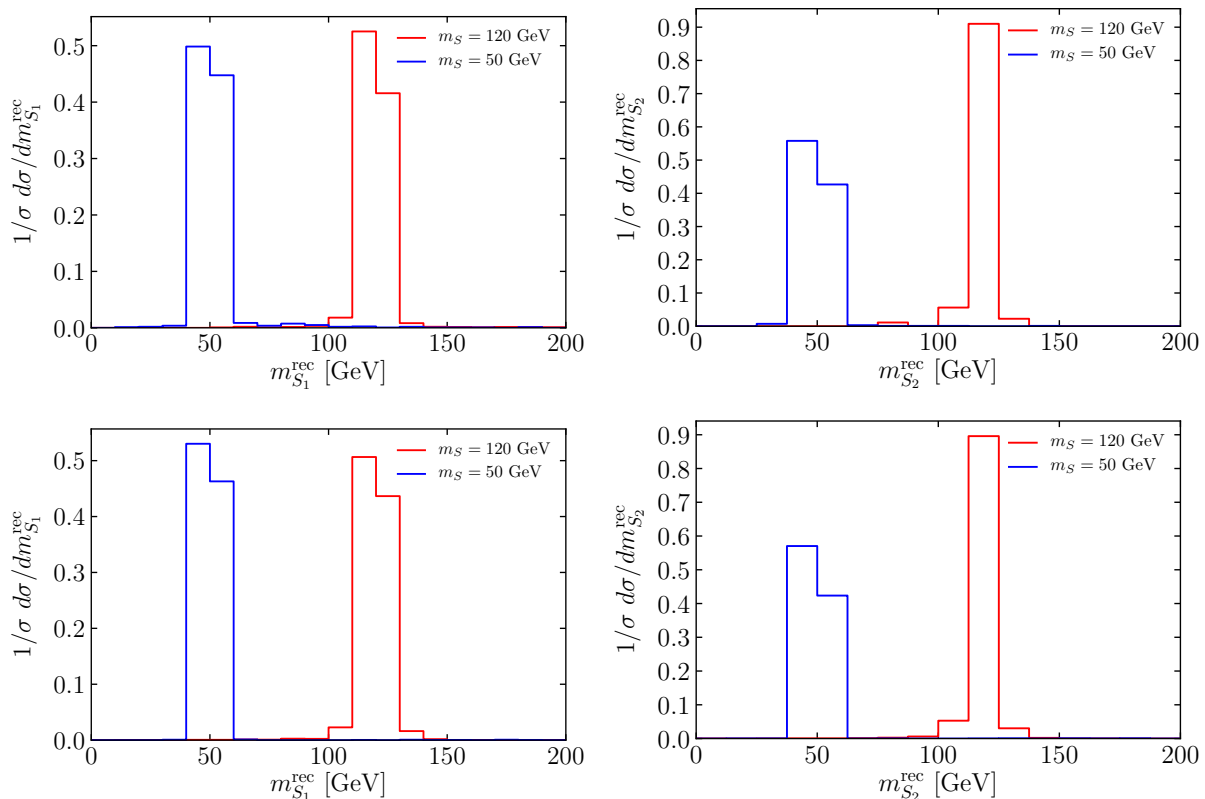


Figure 8: The two reconstructed scalar masses, $m_{S_1}^{\text{rec}}$ and $m_{S_2}^{\text{rec}}$, in the analysis proposed for $t \rightarrow SSq$, $S \rightarrow \mu^+\mu^-$. In the upper (bottom) panel, $q = c$ (u). The distributions assume a collected luminosity of $\mathcal{L} = 150 \text{ fb}^{-1}$.

smaller than 1 TeV. We finally request the $m_{S_{1,2}}^{\text{rec}}$ to be within a window of 30 GeV from the mass of S being probed.

In Figs. 7 and 8, we show the normalized distributions of m_t^{rec} and each m_S^{rec} , respectively, for two signal benchmark points after the basic selection cuts.

The cut flows for the signal are given in Tabs. 9 and 10; in Tab. 11 we show the scalar mass-independent cut flow for the relevant backgrounds. With the final cut on $m_{S_{1,2}}^{\text{rec}}$, the analysis becomes essentially background-free. As before, expected upper limits on the signal strength, $\sigma_{95\%}/\sigma_{\text{th}}$ ($pp \rightarrow tSS(q)$, $S \rightarrow \mu^+\mu^-$), are obtained using the invariant mass of the scalar S candidate distributed into 20 bins. The 95% upper limits on the branching ratio $\mathcal{B}(t \rightarrow SSq, S \rightarrow \mu^+\mu^-)$ and cross section $\sigma(pp \rightarrow tSS(q), S \rightarrow \mu^+\mu^-)$ are shown in Fig. 9, again including the $\pm 1\sigma$ (green band) and the $\pm 2\sigma$ (yellow band) uncertainties.

Cuts/ m_S	20 GeV	30 GeV	40 GeV	50 GeV	60 GeV	70 GeV	80 GeV	90 GeV	100 GeV	120 GeV	150 GeV
Basic	17.77 ± 0.08	15.51 ± 0.07	13.36 ± 0.06	11.53 ± 0.05	10.16 ± 0.05	9.21 ± 0.04	8.53 ± 0.04	2.12 ± 0.02	7.35 ± 0.03	6.36 ± 0.03	5.15 ± 0.02
$n_\ell = 4$	2.87 ± 0.03	2.70 ± 0.03	2.58 ± 0.03	2.47 ± 0.02	2.36 ± 0.02	2.27 ± 0.02	2.25 ± 0.02	1.79 ± 0.02	2.10 ± 0.02	1.94 ± 0.02	1.69 ± 0.01
$n_j \geq 3$	2.47 ± 0.03	2.33 ± 0.03	2.21 ± 0.02	2.10 ± 0.02	2.02 ± 0.02	1.91 ± 0.02	1.89 ± 0.02	0.92 ± 0.01	1.77 ± 0.02	1.63 ± 0.01	1.42 ± 0.01
$n_b = 1$	1.32 ± 0.02	1.20 ± 0.02	1.16 ± 0.02	1.11 ± 0.02	1.04 ± 0.01	1.00 ± 0.01	0.99 ± 0.01	0.92 ± 0.01	0.93 ± 0.01	0.86 ± 0.01	0.736 ± 0.009
$ m_t^{cc} - m_t < 50$ GeV	0.74 ± 0.02	0.68 ± 0.01	0.65 ± 0.01	0.63 ± 0.01	0.58 ± 0.01	0.56 ± 0.01	0.54 ± 0.01	0.509 ± 0.009	0.504 ± 0.009	0.454 ± 0.008	0.393 ± 0.006
$n_{\mu^+\mu^-} = 2$	0.74 ± 0.02	0.68 ± 0.01	0.65 ± 0.01	0.63 ± 0.01	0.58 ± 0.01	0.56 ± 0.01	0.54 ± 0.01	0.509 ± 0.009	0.504 ± 0.009	0.454 ± 0.008	0.393 ± 0.006
$m_{total} < 1$ TeV	0.43 ± 0.01	0.39 ± 0.01	0.38 ± 0.01	0.349 ± 0.009	0.306 ± 0.008	0.281 ± 0.007	0.262 ± 0.007	0.248 ± 0.006	0.238 ± 0.006	0.197 ± 0.005	0.151 ± 0.004
$ m_{S_{1,2}}^{cc} - m_S < 30$ GeV	0.42 ± 0.01	0.39 ± 0.01	0.38 ± 0.01	0.347 ± 0.009	0.301 ± 0.008	0.279 ± 0.007	0.260 ± 0.007	0.245 ± 0.006	0.235 ± 0.006	0.193 ± 0.005	0.146 ± 0.004

Table 9: Event yields after each cut for the eleven benchmark signal points, in the analysis for $t \rightarrow SSu, S \rightarrow \mu^+\mu^-$. We fix $\tilde{Y}_{13} = \tilde{Y}_{31} = 0.1$, $\Lambda = 1$ TeV and $\mathcal{B}(S \rightarrow \mu^+\mu^-) = 1$. The event yields presented assume a collected luminosity of $\mathcal{L} = 150 \text{ fb}^{-1}$.

Cuts/ m_S	20 GeV	30 GeV	40 GeV	50 GeV	60 GeV	70 GeV	80 GeV	90 GeV	100 GeV	120 GeV	150 GeV
Basic cuts	10.19 ± 0.05	7.63 ± 0.04	5.26 ± 0.02	3.43 ± 0.02	2.24 ± 0.01	1.656 ± 0.008	1.447 ± 0.007	0.434 ± 0.004	1.201 ± 0.006	1.000 ± 0.005	0.511 ± 0.003
$n_\ell = 4$	0.76 ± 0.01	0.90 ± 0.01	0.85 ± 0.01	0.729 ± 0.008	0.609 ± 0.006	0.526 ± 0.005	0.495 ± 0.004	0.308 ± 0.003	0.445 ± 0.004	0.395 ± 0.003	0.192 ± 0.002
$n_j \geq 3$	0.68 ± 0.01	0.65 ± 0.01	0.624 ± 0.009	0.520 ± 0.006	0.431 ± 0.005	0.369 ± 0.004	0.350 ± 0.003	0.161 ± 0.002	0.315 ± 0.003	0.281 ± 0.003	0.163 ± 0.001
$n_b = 1$	0.347 ± 0.009	0.356 ± 0.008	0.325 ± 0.006	0.274 ± 0.005	0.227 ± 0.003	0.194 ± 0.003	0.183 ± 0.003	0.161 ± 0.002	0.165 ± 0.002	0.145 ± 0.002	0.083 ± 0.001
$ m_t^{cc} - m_t < 50$ GeV	0.219 ± 0.007	0.151 ± 0.005	0.145 ± 0.004	0.127 ± 0.003	0.105 ± 0.002	0.090 ± 0.002	0.086 ± 0.002	0.046 ± 0.001	0.075 ± 0.001	0.065 ± 0.001	0.046 ± 0.001
$n_{\mu^+\mu^-} = 2$	0.219 ± 0.007	0.151 ± 0.005	0.145 ± 0.004	0.127 ± 0.003	0.105 ± 0.002	0.090 ± 0.002	0.086 ± 0.002	0.046 ± 0.001	0.075 ± 0.001	0.065 ± 0.001	0.046 ± 0.001
$m_{total} < 1$ TeV	0.186 ± 0.007	0.125 ± 0.005	0.123 ± 0.004	0.101 ± 0.003	0.078 ± 0.002	0.062 ± 0.002	0.057 ± 0.001	0.044 ± 0.001	0.048 ± 0.001	0.039 ± 0.001	0.023 ± 0.001
$ m_{S_{1,2}}^{cc} - m_S < 30$ GeV	0.185 ± 0.007	0.121 ± 0.005	0.114 ± 0.004	0.095 ± 0.003	0.074 ± 0.002	0.059 ± 0.002	0.054 ± 0.001	0.044 ± 0.001	0.046 ± 0.001	0.037 ± 0.001	0.022 ± 0.001

Table 10: Event yields after each cut for the eleven benchmark signal points, in the analysis for $t \rightarrow SSq, S \rightarrow \mu^+\mu^-$. We fix $\tilde{Y}_{23} = \tilde{Y}_{32} = 0.1$, $\Lambda = 1$ TeV and $\mathcal{B}(S \rightarrow \mu^+\mu^-) = 1$. The event yields presented assume a collected luminosity of $\mathcal{L} = 150 \text{ fb}^{-1}$.

Cuts/Background	tW	$t\bar{W}/t\bar{Z}$	ZZZ/WWZ	$ZZ/WZ/WW$	$t\bar{t}(\mu)$	tZ
Basic cuts	8084736 ± 36749	649 ± 2	5.28 ± 0.01	14380159 ± 65319	798347 ± 1167	281 ± 1
$n_\ell = 4$	< 42	8.8 ± 0.2	1.372 ± 0.006	1780 ± 727	17 ± 5	0.07 ± 0.02
$n_j \geq 3$	—	5.6 ± 0.2	0.100 ± 0.002	297 ± 297	7 ± 3	0.03 ± 0.01
$n_b = 1$	—	2.6 ± 0.1	0.010 ± 0.001	< 4	3 ± 2	0.011 ± 0.008
$ m_t^{cc} - m_t < 50$ GeV	—	0.62 ± 0.06	0.002 ± 0.001	—	< 2	< 0.006
$n_{\mu^+\mu^-} = 2$	—	0.62 ± 0.06	0.002 ± 0.001	—	—	—
$m_{total} < 1$ TeV	—	0.60 ± 0.06	< 0.0003	—	—	—

Table 11: Event yields after each cut for the dominant backgrounds, in the analysis for $t \rightarrow SSq, S \rightarrow \mu^+\mu^-$. The Z + jets sample is reduced to negligible values after the second cut. The event yields presented assume a collected luminosity of $\mathcal{L} = 150 \text{ fb}^{-1}$.

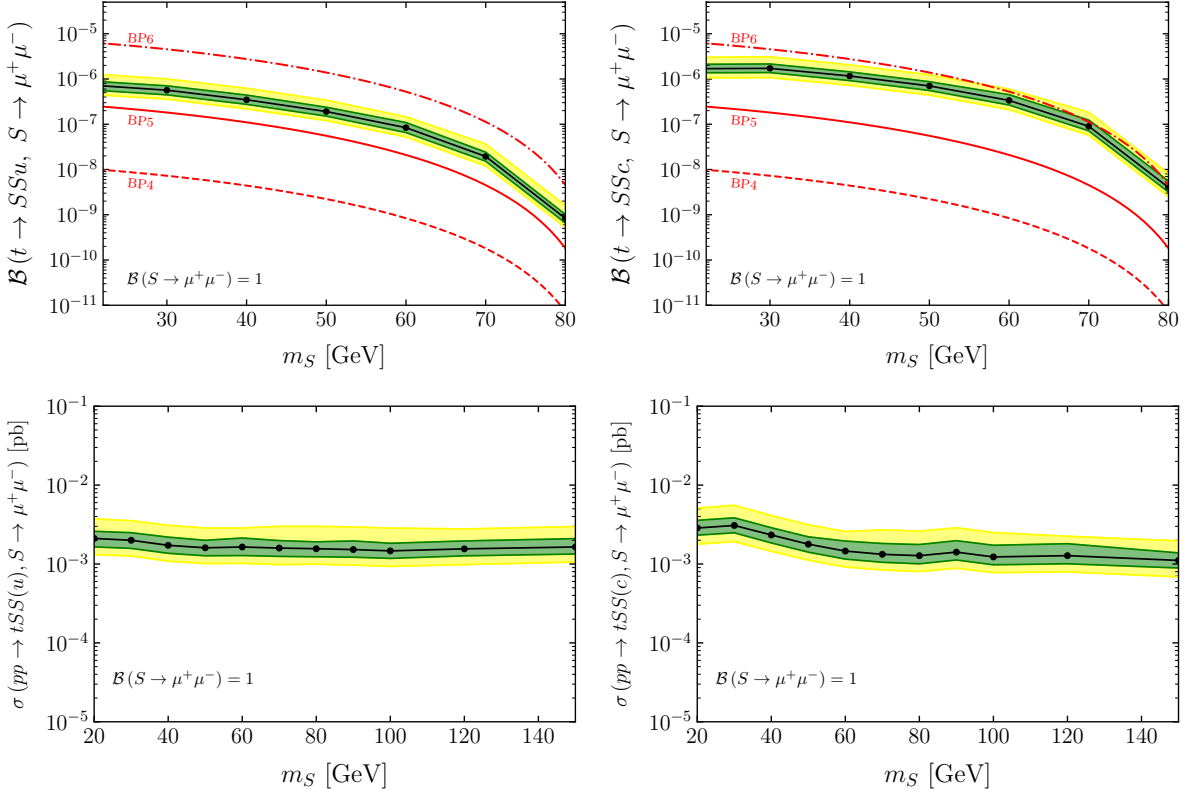


Figure 9: In the upper (bottom) panels, we show the 95% CL limits on the branching ratio (cross section times branching ratio) that can be tested in the $\mu^+\mu^-$ channel, in the analysis proposed for $t \rightarrow SSq$, $S \rightarrow \mu^+\mu^-$, with $q = u$ (c) in the panels on the left (right). The green and yellow bands show the $\pm 1\sigma$ and $\pm 2\sigma$ uncertainty on the limits, respectively. The limits are obtained for a collected luminosity $\mathcal{L} = 150 \text{ fb}^{-1}$. Superimposed are the theoretical expectations in three BPs.

6 Conclusions

Using an effective field theory approach, we have shown that, in models of new physics with light pseudo-scalar singlet degrees of freedom S , new top flavor-changing neutral currents (FCNCs) arise. These can trigger the rare top decay $t \rightarrow Sq$, as well as produce the top quark in association with S in proton-proton collisions. At the LHC, both processes can be captured by inclusive searches for $pp \rightarrow tS + j$.

We have shown that, if there is a \mathbb{Z}_2 symmetry under which S is odd while all the SM quarks are even, then one expects rather the FCNC process $pp \rightarrow tSS + j$. Under this hypothesis, S decays exclusively into leptons, predominantly into taus and muons. For completeness we have shown how these ideas can be implemented in a concrete composite Higgs model. We have also demonstrated that experimental analyses currently performed at the LHC are not significantly sensitive to these interactions. Thus, we have worked

out three new dedicated searches in full detail, including detector simulation and with a rigorous quantification of uncertainties, to probe the processes $pp \rightarrow tS, S \rightarrow \mu^+\mu^-$, $pp \rightarrow tS, S \rightarrow \tau^+\tau^-$ and $pp \rightarrow tSS, S \rightarrow \mu^+\mu^-$.

In the channel $pp \rightarrow tS, S \rightarrow \mu^+\mu^-$ we focus on final state events with three light leptons and jets (with exactly one b -tagged). The main discriminating variable is the invariant mass of the hardest opposite sign muon pair. The dominant background ensues from $t\bar{t}$ and tZ . For an integrated luminosity of 150 fb^{-1} , we find that a production cross section $\sigma(pp \rightarrow tS, S \rightarrow \mu^+\mu^-) > 10^{-3} \text{ pb}$ can be tested at the 95% CL. The highest sensitivity is attained for $m_S \sim 150 \text{ GeV}$, for which we can probe $\mathcal{B}(t \rightarrow Sq) > 5 \text{ (15)} \times 10^{-7}$ at the 95% CL in the up (charm) channel. In turn, for $\mathcal{O}(1)$ couplings in the UV, these results translate into a lower bound on the new physics scale Λ of about 90 TeV, assuming that $\mathcal{B}(S \rightarrow \mu^+\mu^-) = 1$.

In the channel $pp \rightarrow tS, S \rightarrow \tau^+\tau^-$, we focus on final state events with one light lepton and jets (with one b -tagged and two hadronic taus). The main discriminating variable is the invariant mass of the two tau-jets. The dominant backgrounds are $t\bar{t}$ and tW . For an integrated luminosity of 150 fb^{-1} , we find that a production cross section $\sigma(pp \rightarrow tS, S \rightarrow \tau^+\tau^-) > 10^{-2} \text{ pb}$ can be tested at the 95% CL. The highest sensitivity is attained for $m_S \sim 50 \text{ GeV}$, for which we can probe $\mathcal{B}(t \rightarrow Sq) > 11 \text{ (12)} \times 10^{-6}$ at the 95% CL in the up (charm) channel. In turn, for $\mathcal{O}(1)$ couplings in the UV, these results translate into a lower bound on the new physics scale Λ of about 75 TeV, assuming that $\mathcal{B}(S \rightarrow \tau^+\tau^-) = 1$.

For $pp \rightarrow tSS, S \rightarrow \mu^+\mu^-$, we concentrate on events with four light leptons and jets (one of which b -tagged). The principal discriminating variable is the invariant mass of the four leptons. This search is in good approximation background free. For an integrated luminosity of 150 fb^{-1} , we find that a production cross section $\sigma(pp \rightarrow tSS, S \rightarrow \mu^+\mu^-) > 10^{-3} \text{ pb}$ can be tested at 95% CL. In the small mass regime, we can probe $\mathcal{B}(t \rightarrow SSq) > 10^{-6}$ at the 95% CL. The strongest limits in branching ratio are obtained for $m_S \sim 80 \text{ GeV}$, for which we can probe $\mathcal{B}(t \rightarrow SSq) > 5 \text{ (25)} \times 10^{-10}$ in the up (charm) channel. In turn, for $\mathcal{O}(1)$ couplings in the UV, these results translate into a lower bound on the new physics scale Λ of about 2 TeV, assuming that $\mathcal{B}(S \rightarrow \mu^+\mu^-) = 1$.

Naive prospects for higher luminosities can be obtained by scaling the statistical significance with $\sqrt{\mathcal{L}}$. Thus, at $\mathcal{L} = 3 \text{ ab}^{-1}$, we expect to probe scales of order 200, 160, and 3 TeV in each of the channels, respectively.

Acknowledgements

The authors were partially funded by FCT - Fundação para a Ciência e a Tecnologia, I.P., Portugal, under projects CERN/FIS-PAR/0024/2019 (MC, NC and MR) and CERN/FIS-PAR/0002/2019 (NC and AP). MC is also supported by the Spanish MINECO under the Juan de la Cierva programme as well as by the Ministry of Science and Innovation under grant numbers FPA2016-78220-C3-3-P (fondos FEDER), and by the Junta de Andalucía grants FQM 101 and A-FQM-211-UGR-18 (fondos FEDER). AP acknowledges the support by FCT through grant SFRH/BD/129321/2017. MR acknowledges support by FCT

under the grant PD/BD/142773/2018 and by LIP (FCT, COMPETE2020-Portugal2020, FEDER, POCI-01-0145-FEDER-007334). The computational part of this work was supported by INCD (funded by FCT and FEDER under the project 01/SAICT/2016 nr. 022153) and by the Minho Advanced Computing Center (MACC).

References

- [1] U. Ellwanger, C. Hugonie and A. M. Teixeira, *The Next-to-Minimal Supersymmetric Standard Model*, *Phys. Rept.* **496** (2010) 1–77, [[0910.1785](#)].
- [2] R. Contino, Y. Nomura and A. Pomarol, *Higgs as a holographic pseudoGoldstone boson*, *Nucl. Phys. B* **671** (2003) 148–174, [[hep-ph/0306259](#)].
- [3] B. Gripaios, A. Pomarol, F. Riva and J. Serra, *Beyond the Minimal Composite Higgs Model*, *JHEP* **04** (2009) 070, [[0902.1483](#)].
- [4] M. Chala, *$h \rightarrow \gamma\gamma$ excess and Dark Matter from Composite Higgs Models*, *JHEP* **01** (2013) 122, [[1210.6208](#)].
- [5] L. Vecchi, *The Natural Composite Higgs*, [1304.4579](#).
- [6] B. Bellazzini, C. Cski and J. Serra, *Composite Higgses*, *Eur. Phys. J. C* **74** (2014) 2766, [[1401.2457](#)].
- [7] V. Sanz and J. Setford, *Composite Higgses with seesaw EWSB*, *JHEP* **12** (2015) 154, [[1508.06133](#)].
- [8] T. Ma and G. Cacciapaglia, *Fundamental Composite 2HDM: $SU(N)$ with 4 flavours*, *JHEP* **03** (2016) 211, [[1508.07014](#)].
- [9] A. Belyaev, G. Cacciapaglia, H. Cai, T. Flacke, A. Parolini and H. Serdio, *Singlets in composite Higgs models in light of the LHC 750 GeV diphoton excess*, *Phys. Rev. D* **94** (2016) 015004, [[1512.07242](#)].
- [10] M. Chala, G. Nardini and I. Sobolev, *Unified explanation for dark matter and electroweak baryogenesis with direct detection and gravitational wave signatures*, *Phys. Rev. D* **94** (2016) 055006, [[1605.08663](#)].
- [11] B. Gripaios, M. Nardecchia and T. You, *On the Structure of Anomalous Composite Higgs Models*, *Eur. Phys. J. C* **77** (2017) 28, [[1605.09647](#)].
- [12] M. Chala, R. Grober and M. Spannowsky, *Searches for vector-like quarks at future colliders and implications for composite Higgs models with dark matter*, *JHEP* **03** (2018) 040, [[1801.06537](#)].
- [13] M. Chala, R. Grober and M. Spannowsky, *Interplay between collider searches for vector-like quarks and dark matter searches in composite Higgs models*, *Int. J. Mod. Phys. A* **34** (2019) 1940011.

- [14] G. Cacciapaglia, G. Ferretti, T. Flacke and H. Serdio, *Light scalars in composite Higgs models*, *Front. in Phys.* **7** (2019) 22, [[1902.06890](#)].
- [15] M. Ramos, *Non-Minimal Composite Dark Matter*, [1912.11061](#).
- [16] J. R. Espinosa, B. Gripaios, T. Konstandin and F. Riva, *Electroweak Baryogenesis in Non-minimal Composite Higgs Models*, *JCAP* **01** (2012) 012, [[1110.2876](#)].
- [17] V. Vaskonen, *Electroweak baryogenesis and gravitational waves from a real scalar singlet*, *Phys. Rev. D* **95** (2017) 123515, [[1611.02073](#)].
- [18] A. Beniwal, M. Lewicki, J. D. Wells, M. White and A. G. Williams, *Gravitational wave, collider and dark matter signals from a scalar singlet electroweak baryogenesis*, *JHEP* **08** (2017) 108, [[1702.06124](#)].
- [19] Z. Kang, P. Ko and T. Matsui, *Strong first order EWPT & strong gravitational waves in Z_3 -symmetric singlet scalar extension*, *JHEP* **02** (2018) 115, [[1706.09721](#)].
- [20] B. Grzadkowski and D. Huang, *Spontaneous CP-Violating Electroweak Baryogenesis and Dark Matter from a Complex Singlet Scalar*, *JHEP* **08** (2018) 135, [[1807.06987](#)].
- [21] S. De Curtis, L. Delle Rose and G. Panico, *Composite Dynamics in the Early Universe*, *JHEP* **12** (2019) 149, [[1909.07894](#)].
- [22] J. Liu, C. E. M. Wagner and X.-P. Wang, *A light complex scalar for the electron and muon anomalous magnetic moments*, *JHEP* **03** (2019) 008, [[1810.11028](#)].
- [23] N. Craig, H. K. Lou, M. McCullough and A. Thalappilil, *The Higgs Portal Above Threshold*, *JHEP* **02** (2016) 127, [[1412.0258](#)].
- [24] C. Baker et al., *An Improved experimental limit on the electric dipole moment of the neutron*, *Phys. Rev. Lett.* **97** (2006) 131801, [[hep-ex/0602020](#)].
- [25] ACME collaboration, V. Andreev et al., *Improved limit on the electric dipole moment of the electron*, *Nature* **562** (2018) 355–360.
- [26] R. Franceschini, G. F. Giudice, J. F. Kamenik, M. McCullough, F. Riva, A. Strumia et al., *Digamma, what next?*, *JHEP* **07** (2016) 150, [[1604.06446](#)].
- [27] B. Gripaios and D. Sutherland, *An operator basis for the Standard Model with an added scalar singlet*, *JHEP* **08** (2016) 103, [[1604.07365](#)].
- [28] S. Banerjee, M. Chala and M. Spannowsky, *Top quark FCNCs in extended Higgs sectors*, *Eur. Phys. J.* **C78** (2018) 683, [[1806.02836](#)].
- [29] J. Aguilar-Saavedra and G. Branco, *Probing top flavor changing neutral scalar couplings at the CERN LHC*, *Phys. Lett. B* **495** (2000) 347–356, [[hep-ph/0004190](#)].

- [30] D. Atwood, S. K. Gupta and A. Soni, *Constraining the flavor changing Higgs couplings to the top-quark at the LHC*, *JHEP* **10** (2014) 057, [[1305.2427](#)].
- [31] A. Papaefstathiou and G. Tetlalmatzi-Xolocotzi, *Rare top quark decays at a 100 TeV proton–proton collider: $t \rightarrow bWZ$ and $t \rightarrow hc$* , *Eur. Phys. J. C* **78** (2018) 214, [[1712.06332](#)].
- [32] ATLAS collaboration, M. Aaboud et al., *Search for top quark decays $t \rightarrow qH$, with $H \rightarrow \gamma\gamma$, in $\sqrt{s} = 13$ TeV pp collisions using the ATLAS detector*, *JHEP* **10** (2017) 129, [[1707.01404](#)].
- [33] ATLAS collaboration, M. Aaboud et al., *Search for flavor-changing neutral currents in top quark decays $t \rightarrow Hc$ and $t \rightarrow Hu$ in multilepton final states in proton-proton collisions at $\sqrt{s} = 13$ TeV with the ATLAS detector*, *Phys. Rev. D* **98** (2018) 032002, [[1805.03483](#)].
- [34] M. Chala, J. Santiago and M. Spannowsky, *Constraining four-fermion operators using rare top decays*, *JHEP* **04** (2019) 014, [[1809.09624](#)].
- [35] M. Barros, N. F. Castro, J. Erdmann, G. Gener, K. Krninger, S. La Cagnina et al., *Study of interference effects in the search for flavour-changing neutral current interactions involving the top quark and a photon or a Z boson at the LHC*, *Eur. Phys. J. Plus* **135** (2020) 339, [[1909.08443](#)].
- [36] CMS collaboration, V. Khachatryan et al., *Search for Higgs boson off-shell production in proton-proton collisions at 7 and 8 TeV and derivation of constraints on its total decay width*, *JHEP* **09** (2016) 051, [[1605.02329](#)].
- [37] CMS collaboration, A. M. Sirunyan et al., *Search for low-mass resonances decaying into bottom quark-antiquark pairs in proton-proton collisions at $\sqrt{s} = 13$ TeV*, *Phys. Rev. D* **99** (2019) 012005, [[1810.11822](#)].
- [38] CMS collaboration, A. M. Sirunyan et al., *Search for high mass dijet resonances with a new background prediction method in proton-proton collisions at $\sqrt{s} = 13$ TeV*, *JHEP* **05** (2020) 033, [[1911.03947](#)].
- [39] R. Harnik, J. Kopp and J. Zupan, *Flavor Violating Higgs Decays*, *JHEP* **03** (2013) 026, [[1209.1397](#)].
- [40] UTFIT collaboration, M. Bona et al., *Model-independent constraints on $\Delta F = 2$ operators and the scale of new physics*, *JHEP* **03** (2008) 049, [[0707.0636](#)].
- [41] TOP QUARK WORKING GROUP collaboration, K. Agashe et al., *Working Group Report: Top Quark*, in *Community Summer Study 2013: Snowmass on the Mississippi*, 11, 2013. [1311.2028](#).
- [42] PARTICLE DATA GROUP collaboration, M. Tanabashi et al., *Review of Particle Physics*, *Phys. Rev. D* **98** (2018) 030001.

- [43] D. B. Kaplan and H. Georgi, *SU(2) x U(1) Breaking by Vacuum Misalignment*, *Phys. Lett. B* **136** (1984) 183–186.
- [44] D. B. Kaplan, H. Georgi and S. Dimopoulos, *Composite Higgs Scalars*, *Phys. Lett. B* **136** (1984) 187–190.
- [45] ATLAS collaboration, M. Aaboud et al., *Search for flavour-changing neutral current top-quark decays $t \rightarrow qZ$ in proton-proton collisions at $\sqrt{s} = 13$ TeV with the ATLAS detector*, *JHEP* **07** (2018) 176, [[1803.09923](#)].
- [46] R. Brun and F. Rademakers, *ROOT: An object oriented data analysis framework*, *Nucl. Instrum. Meth. A* **389** (1997) 81–86.
- [47] M. Cacciari, G. P. Salam and G. Soyez, *FastJet User Manual*, *Eur. Phys. J. C* **72** (2012) 1896, [[1111.6097](#)].
- [48] J. Alwall, R. Frederix, S. Frixione, V. Hirschi, F. Maltoni, O. Mattelaer et al., *The automated computation of tree-level and next-to-leading order differential cross sections, and their matching to parton shower simulations*, *JHEP* **07** (2014) 079, [[1405.0301](#)].
- [49] T. Sjöstrand, S. Ask, J. R. Christiansen, R. Corke, N. Desai, P. Ilten et al., *An Introduction to PYTHIA 8.2*, *Comput. Phys. Commun.* **191** (2015) 159–177, [[1410.3012](#)].
- [50] M. Czakon and A. Mitov, *Top++: A Program for the Calculation of the Top-Pair Cross-Section at Hadron Colliders*, *Comput. Phys. Commun.* **185** (2014) 2930, [[1112.5675](#)].
- [51] ATLAS collaboration, M. Aaboud et al., *Search for supersymmetry in events with four or more leptons in $\sqrt{s} = 13$ TeV pp collisions with ATLAS*, *Phys. Rev. D* **98** (2018) 032009, [[1804.03602](#)].
- [52] A. Alloul, N. D. Christensen, C. Degrande, C. Duhr and B. Fuks, *Feynrules 2.0 a complete toolbox for tree-level phenomenology*, *Computer Physics Communications* **185** (Aug, 2014) 22502300.
- [53] R. D. Ball, V. Bertone, S. Carrazza, C. S. Deans, L. D. Debbio], S. Forte et al., *Parton distributions with lhc data*, *Nuclear Physics B* **867** (2013) 244 – 289.
- [54] J. de Favereau, C. Delaere, P. Demin, A. Giammanco, V. Lematre, A. Mertens et al., *Delphes 3: a modular framework for fast simulation of a generic collider experiment*, *Journal of High Energy Physics* **2014** (Feb, 2014) .
- [55] M. Cacciari, G. P. Salam and G. Soyez, *The anti- k_t jet clustering algorithm*, *JHEP* **04** (2008) 063, [[0802.1189](#)].

- [56] A. L. Read, *Presentation of search results: the CL_s technique*, *J. Phys. G* **28** (2002) 2693–704.
- [57] E. Busato, D. Calvet and T. Theveneaux-Pelzer, *OpTHyLiC: an Optimised Tool for Hybrid Limits Computation*, *Comput. Phys. Commun.* **226** (2018) 136–150, [[1502.02610](#)].